

COVER PAGE

Document downloaded by @DAEL

Sun Nov 22 13:30:30 2026
For personal use

When automatic English translation is provided, only the original document is authentic.
The EAA cannot be held responsible of any translation error

Bibliographical reference

Scattering and Absorption of Sound by a Compound Cylindrical Porous Absorber with an Eccentric Core, Seyyed M. Hasheminejad and Siavash Kazemirad, Acta Acustica **vol. 94** (Number 1), 2008, pp. 79-90

DOI
https://doi.org/10.3813/AAA.918011

Acta Acustica united with Acustica
Vol. 94 (2008) 79 – 90

DOI 10.3813/AAA.918011

Scattering and Absorption of Sound by a Compound Cylindrical Porous Absorber with an Eccentric Core

Seyyed M. Hasheminejad, Siavash Kazemirad
Acoustics Research Lab., Department of Mechanical Engineering, Iran University of Science and Technology, Narmak, Tehran 16844, Iran. hashemi@iust.ac.ir

Summary
The classical method of separation of variables along with the novel features of Biot theory of dynamic poroelasticity and the translational addition theorem for cylindrical wave functions are employed to present an exact solution for interaction of a plane acoustic wave with a composite cylindrical sound absorber suspended in air. The analytical results are illustrated with numerical examples in which a compound cylindrical absorber made of selected configurations of two common sound absorbent materials (plastic foam and light glass wool), is insonified by plane sound waves at selected angles of incidence. The backscattered form function amplitude as well as the absorption cross section spectra are calculated and discussed for representative values of the parameters characterizing the system. The effects of incident wave frequency, angle of incidence, core eccentricity and coating thickness are examined. Limiting cases are considered and fair agreements with available solutions are obtained.

PACS no. 43.55.Ev, 43.20.Gp, 43.50.Gf

1. Introduction

The problem of acoustic diffraction by an object has attracted the attention of numerous researchers since the late 19th century. In particular, sound wave scattering by cylindrical objects has been investigated quite extensively since works of Rayleigh [1] and Lamb [2]. For example, the scattering of acoustic waves has been broadly studied for a rigid, fixed, solid circular cylinder [3], for solid elastic and viscoelastic circular cylinders [4, 5], for elastic and viscoelastic cylindrical shells [6, 7], for viscoelastically coated cylinders [8], and for cylindrical objects with permeable or impedance boundary condition [9, 10, 11, 12, 13, 14, 15]. Several authors have investigated acoustic scattering from a permeable (an impedance) cylindrical obstacle in an unbounded fluid medium. Shaw [9] used a boundary integral equation approach to study scattering of plane time-harmonic waves by a circular cylinder with variable boundary impedance. Mechel [10] employed Series of Bessel functions to calculate absorption and scattering cross sections of porous cylindrical absorbers. Scattering of sound waves by a fluid-saturated porous cylinder is examined by Laperre and Thys [11]. The steady state scattering of compressional wave by an absorbing cylinder is also studied by Liu [12]. Zhou *et al.* [13] used the Biot-Stoll's theory, which accounts for the viscosity of fluid and the inelastic loss of solid skeleton, to examine sound scattering by fluid-saturated porous cylinders. The scattering of sound from a cylinder with locally varying surface impedance, using a variant of the generalized minimum residual (GMRES) method is studied by Ochmann *et al.* [14]. Sarradj [15] presented a multidomain boundary element method for calculation of sound fields in and around a cylinder of porous absorber material having a rigid frame. In a closely related problem, Berryman [16] studied ultrasonic dispersion of extensional waves in fluid-saturated porous cylinders with open-pore surface and closed-pore surface boundary conditions by analyzing generalized Pochhammer equations derived using Biot's theory of wave propagation in fluid-saturated porous media. Also, Reddy and Tajuddin [17] used Biot's theory to study the plane-strain vibrations of thick walled hollow, composite poroelastic cylinders with pervious and impervious boundary conditions.

Analytical solutions of interior or exterior boundary value problems in various fields such as potential theory, acoustics and electromagnetism, are strictly dependent on the shape of boundaries. In particular, when multiple interfaces are present in a sound field, there is an acoustical interaction between them due to cross scattering. Several researchers have studied the acoustic interaction problems involving multiple cylindrical boundaries. Shaw and Tai [18] used Helmholtz integral equation formulation to study acoustic radiation due to a time harmonic pressure applied at the inner boundary of an acoustic fluid body composed of two parallel, nonconcentric circular cylin-

Received 14 June 2007,
accepted 6 August 2007.

© S. Hirzel Verlag · EAA

Document downloaded by @DAEL, 2026-11-22 13:30:33 - personal use only

ders. Kanevskii and Surikov [19] theoretically and experimentally investigated the field in the focal plane of cylindrical two-layer acoustic lenses formed by two concentric layers with different refractive indices. Reese and Thompson [20] used the translational addition theorem for cylindrical wave functions to investigate the effect of a variable thickness, cylindrical, fluid layer on the directional response patterns of a particular acoustic source distribution. Poruchikov and Stepanov [21] examined the effect of acoustic waves on a rigid immobile infinite cylinder covered with a thin compressible coating and immersed in an unbounded fluid. Sinai and Waag [22] employed a series solution for scattering from two concentric fluid cylinders to compute the scattered pressure for a range of frequencies and material parameters. Schuster [23] presented a fast exact numerical algorithm that computes the line source acoustic response of concentric cylinders filled with acoustic material of contrasting impedances. Janele *et al.* [24] considered the finite amplitude wave propagation which results when a compound cylinder consisting of two concentric, isotropic compressible cylinders is subjected to a sudden spatially uniform application of pressure at the inner cylinder's surface. Morse *et al.* [25] showed that scattering by a nonconcentric circular cylinder exhibits scattering processes not present in the simple case of uniform thickness. Roumeliotis and Kakogiannos [26] used the translational addition theorems for cylindrical wave functions to study scattering of an acoustic plane wave from an infinite circular impenetrable or penetrable cylinder of an acoustically small radius, embedded eccentrically into a penetrable cylinder. Danila *et al.* [27, 28] used the generalized Debye series expansion (GDSE) method for calculation of the scattered field due to a plane wave incident on concentric or eccentric fluid-solid cylindrical interfaces. Hasheminejad and Azarpeyvand [29] presented an exact analysis of acoustic radiation from a vibrating cylindrical source eccentrically suspended within a fluid cylinder. Umnova *et al.* [30] used an extended multiple scattering model to both theoretically and experimentally study the acoustic transmission loss of a finite periodic array of long rigid cylinders, with and without porous absorbent covering. In a closely related problem, Hasheminejad and Avazmohammadi [31] used the novel features of Biot theory of poroelasticity along with translational addition theorem for cylindrical wave functions to study interaction of a plane acoustic wave with a pair of air-saturated poroelastic cylindrical absorbers suspended in air. Also, Zhong and Wang [32] presented theoretical investigations on solitary waves interacting with a surface-piercing concentric porous cylinder system, where the outer cylinder is porous and considered thin in thickness, while the inner cylinder is solid.

The above review clearly indicates that while there exists a vast body of literature on acoustic wave scattering from a solid permeable cylindrical obstacle, rigorous analytic or numerical solutions involving a compound cylindrical absorber seem to be nonexistent. To fill this gap, we employ the novel features of Biot dynamic theory of poroelasticity along with the translation addition theorem for cylindrical wave functions to formulate an exact analysis for scattering of acoustic plane waves by a compound air-saturated porous elastic cylindrical sound absorber suspended in air (Figure 1). The proposed model is of noble interest essentially due to its inherent value as a canonical problem in structural acoustics and noise control engineering. It can form an invaluable guide in forming the basis for assessment of effect of the composite absorber core eccentricity and coating thickness on the scattered sound field. The presented exact solution has promising applications in a wide range of physical and technical fields including design of sound absorptive noise control systems [10], ultrasonic characterization of porous coated cylindrical implants [33, 34, 35, 36], ultrasonic testing of porous coatings for passive control of bluff body flows [37] and hypersonic boundary-layer stability [38], and design of shock-absorbing ultrasonically absorptive coatings [39]. It can also serve as the benchmark for comparison to other solutions obtained by strictly numerical or asymptotic approaches.

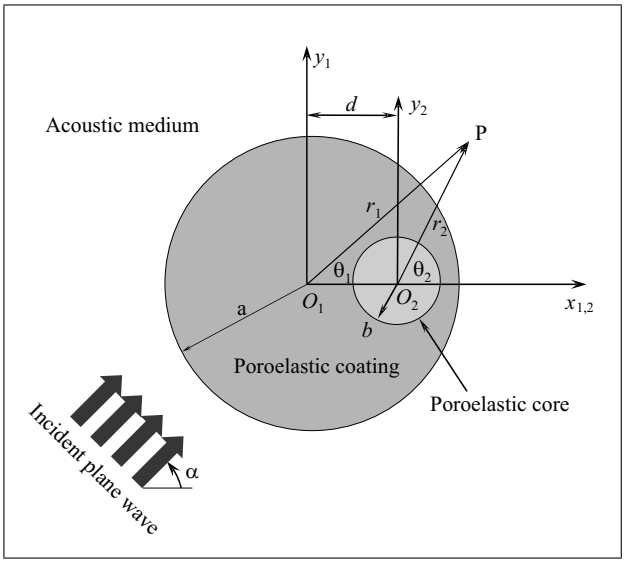


Figure 1. Problem geometry.

2. Formulation

2.1. Acoustic field equations

Here, we theoretically examine the two-dimensional scattered acoustic field produced by a plane compressional wave normally incident on a compound poroelastic cylinder defined by two nonconcentric cylindrical surfaces of radii "a" and b immersed in an ideal boundless acoustic medium. The problem geometry is shown in Figure 1. Two polar coordinate systems $(r_i, \theta_i; i = 1, 2)$ are introduced to describe the different acoustic fields inside the compound cylinder. The cylinder axes extend to infinity and are parallel. Their origin-to-origin separation is d, and point P is an arbitrary field point outside the compound cylinder. The problem can be analyzed by means of the standard meth-

Document downloaded by @DAEL, 2026-11-22 13:30:33 - personal use only

ods of theoretical acoustics. The fluid is assumed to be an inviscid and ideal compressible medium that cannot support shear stresses. Hence, the state of stress in the fluid is purely hydrostatic and the field equations may conveniently be expressed in terms of a scalar velocity potential as

$$\dot{\boldsymbol{s}} = \nabla\varphi, \quad p = -\rho_0\dot{\varphi}, \quad \nabla^2\varphi + k^2\varphi = 0, \tag{1}$$

where $k = \omega/c_0$ is the wave number for the dilatational wave, ρ_0 is the fluid density, $\dot{\boldsymbol{s}}$ is the fluid particle velocity vector, p is the acoustic pressure and c_0 is the speed of sound in the fluid. In view of the fact that the incident wave is time-harmonic, with the circular frequency ω, we shall assume harmonic time variations throughout with the $\mathrm{e}^{-\mathrm{i}\omega t}$ dependence suppressed for simplicity.

The dynamics of the problem may be expressed in terms of appropriate scalar potentials that can be represented in the form of an infinite generalized Fourier series whose unknown scattering coefficients are to be determined by imposing the proper boundary conditions. The incident wave in the cylindrical coordinate system of the outer cylinder (r_1, θ_1) may be written in the standard form [3]

$$\varphi_{\mathrm{inc}}(r_1, \theta_1, \omega) = \varphi_0 \sum_{n=-\infty}^{\infty} \mathrm{i}^n J_n(kr_1)\mathrm{e}^{\mathrm{i}n(\theta_1-\alpha)}, \tag{2}$$

where φ_0 is amplitude of the incident wave, α is the angle of incidence, and J_n is the cylindrical Bessel function of the first kind [40]. Furthermore, the acoustic field scattered by the compound cylinder, is conveniently expressed in the form

$$\varphi_{\mathrm{scat}}(r_1, \theta_1, \omega) = \sum_{n=-\infty}^{\infty} A_n(\omega)H_n(kr_1)\mathrm{e}^{\mathrm{i}n\theta_1}, \tag{3}$$

where $A_n(\omega)$ are unknown scattering coefficients and $H_n(x) = J_n(x) + \mathrm{i}Y_n(x)$ is the cylindrical Hankel function of order n [40], and the total acoustic potential $\varphi = \varphi_{\mathrm{inc}} + \varphi_{\mathrm{scat}}$ satisfies field equations (1).

2.2. Poroelastic model

On a microscopic scale, sound propagation in porous materials is generally difficult to study due to the complicated geometries of the frames. In Biot model the medium is taken to be a macroscopically homogeneous and isotropic two-component solid/fluid system with the same macroscopic bulk properties as the real porous material. Denoting the average macroscopic displacement of the solid frame and the saturating fluid on the elementary macroscopic volume (EMV) by the vectors $\boldsymbol{u}$ and $\boldsymbol{U}$, respectively, and assuming harmonic time dependence $\mathrm{e}^{-\mathrm{i}\omega t}$, the equation of motion can be written in the form [41]

$$\begin{aligned} &P\nabla\big(\nabla\cdot\boldsymbol{u}\big) - N\nabla\times\big(\nabla\times\boldsymbol{u}\big) \\ &\qquad +Q\nabla\big(\nabla\cdot\boldsymbol{U}\big) + \omega^2\big(\overline{\rho}_{11}\boldsymbol{u} + \overline{\rho}_{12}\boldsymbol{U}\big) = 0, \\ &Q\nabla\big(\nabla\cdot\boldsymbol{u}\big) + R\nabla\times\big(\nabla\times\boldsymbol{u}\big) + \omega^2\big(\overline{\rho}_{12}\boldsymbol{u} + \overline{\rho}_{22}\boldsymbol{U}\big) = 0. \end{aligned} \tag{4}$$

In these equations, N is the shear modulus of the frame in vacuum, P, Q and R are generalized elastic constants which will be defined later, and the equivalent mass density coefficients $\overline{\rho}_{11}(\omega)$, $\overline{\rho}_{12}(\omega)$ and $\overline{\rho}_{22}(\omega)$, which account for inertial and viscous coupling between the solid and fluid phases, are defined as

$$\begin{aligned} \overline{\rho}_{11}(\omega) &= \rho_{11} + \mathrm{i}\sigma\phi_0^2 G_J(\omega)/\omega, \\ \overline{\rho}_{12}(\omega) &= \rho_{12} - \mathrm{i}\sigma\phi_0^2 G_J(\omega)/\omega, \\ \overline{\rho}_{22}(\omega) &= \rho_{22} + \mathrm{i}\sigma\phi_0^2 G_J(\omega)/\omega, \end{aligned} \tag{5}$$

where $\rho_{11} = \rho_1 + \rho_a$, $\rho_{12} = -\rho_a$, $\rho_{22} = \phi_0\rho_0 + \rho_a$, $\rho_a = \phi_0\rho_0(\alpha_\infty - 1)$ in which ϕ_0 and α_∞ are porosity and tortuosity of the porous material, respectively, and having adopted the simple model presented by Johnson *et al.* [42] for description of the dynamic permeability effects, the dynamic viscosity correction factor $G_J(\omega)$ is given as

$$G_J(\omega) = \sqrt{1 - \mathrm{i}\frac{4\alpha_\infty^2\eta\rho_0\omega}{\sigma^2\Lambda^2\phi_0^2}}, \tag{6}$$

where σ is flow resistivity of the porous material, η is the shear (dynamic) viscosity, and the viscous characteristic length is determined from $\Lambda \approx \sqrt{8\alpha_\infty\eta/\phi_0}/c$, in which c is a shape factor whose order of magnitude lies between 0.3 and 3.0 for most materials. Moreover, the generalized elastic constants P, Q and R are expressed as

$$\begin{aligned} P &= \frac{4}{3}N + K_b + \frac{(1-\phi_0)^2}{\phi_0}K_f, \\ Q &= K_f(1-\phi_0), \qquad R = K_f\phi_0, \end{aligned} \tag{7}$$

where $K_b = 2N(\nu+1)/[3(1-2\nu)]$ is bulk modulus of the porous skeletal frame and ν is Poisson ratio. Furthermore, the complex bulk modulus for air-saturated porous materials is written as [41]

$$K_f(\omega = \gamma p_0\left[\gamma - (\gamma-1)\Big(1 - \frac{\sigma'\phi_0}{\mathrm{i}\omega Pr^2\rho_0\alpha_\infty}G_J'(Pr^2\omega)\Big)^{-1}\right]^{-1}, \tag{8}$$

where p_0 is the ambient pressure, γ is the specific heat ratio, Pr is Prandtl number and $G_J'(\omega)$ is the dynamic thermal correction factor which is given by

$$G_J'(Pr^2\omega) = \sqrt{1 - \mathrm{i}\frac{4\alpha_\infty^2\eta\rho_0\omega Pr^2}{\sigma'^2\Lambda'^2\phi_0^2}}, \tag{9}$$

in which the thermal characteristic length is determined from $\Lambda' \approx \sqrt{8\alpha_\infty\eta/\phi_0\sigma}/c'$, where $c' = \sqrt{\sigma'/\sigma}$ is a coefficient that is smaller or equal to c [42].

Next, in the absence of body forces, the displacements $\boldsymbol{u}$ and $\boldsymbol{U}$ can respectively be decomposed as the superposition of longitudinal and transverse vector components in the form [41]:

$$\boldsymbol{u} = \nabla\phi^s + \nabla\times\boldsymbol{\psi}^s, \quad \boldsymbol{U} = \nabla\phi^f + \nabla\times\boldsymbol{\psi}^f, \tag{10}$$

Document downloaded by @DAEL, 2026-11-22 13:30:33 - personal use only

where, noting the two-dimensional nature of the problem (i.e., the translational invariance of the incident field along the z-axis of the compound cylinder; see Figure 1), we may adopt the simplifying assumption $\boldsymbol{\psi}^{s,f} = (0, 0, \psi^{s,f})$ [43]. Subsequent incorporation of the above resolutions into Biot's field equations of motion (4), after solving the corresponding eigenvalue problem, leads to the Helmholtz type equations [41]:

$$\nabla^2\phi^s_{1,2} + k^2_{1,2}\phi^s_{1,2} = 0, \qquad \nabla^2\psi^s + k^2_3\psi^s = 0, \quad (11)$$

where ∇^2 is the Laplacian and the propagation constants k_1 and k_2, which characterize two compressional waves (i.e., the so called "solid-borne" and the "fluid-borne" waves), are found from

$$k^2_{1,2} = \frac{\omega^2}{2(PR-Q^2)}\left(P\overline{\rho}_{22} + R\overline{\rho}_{11} - 2Q\overline{\rho}_{12} \mp \sqrt{\Delta}\right), \quad (12)$$

with $\Delta = (P\overline{\rho}_{22} + R\overline{\rho}_{11} - 2Q\overline{\rho}^2_{12})^2 - 4(PR-Q^2)(\overline{\rho}_{11}\overline{\rho}_{22} - \overline{\rho}^2_{12})$. Moreover, the ratio μ_i between displacement of fluid and solid phases (i.e., the so called compatibility coefficients) for each wave is given by [41]

$$\mu_i = \frac{\phi^f_i}{\phi^s_i} = \frac{Pk^2_i - \omega^2\overline{\rho}_{11}}{\omega^2\overline{\rho}_{12} - Qk^2_i}, \quad i = 1, 2. \quad (13)$$

Similarly, the propagating shear wave in the poroelastic medium is characterized by

$$k^2_3 = \frac{\omega^2}{N}\frac{\overline{\rho}_{11}\overline{\rho}_{22} - \overline{\rho}^2_{12}}{\overline{\rho}_{22}}, \quad \mu_3 = \frac{\psi^f}{\psi^s} = -\frac{\overline{\rho}_{12}}{\overline{\rho}_{22}}. \quad (14)$$

Next, considering the fundamental field equations in the general cylindrical coordinates, the solid and fluid displacements in terms of displacement potentials are written as [44]

$$\begin{aligned} u_r &= \frac{\partial\phi^s}{\partial r} + \frac{1}{r}\frac{\partial\psi^s}{\partial\theta}, \quad U_r = \frac{\partial\phi^f}{\partial r} + \frac{1}{r}\frac{\partial\psi^f}{\partial\theta}, \\ u_\theta &= \frac{1}{r}\frac{\partial\phi^s}{\partial\theta} - \frac{\partial\psi^s}{\partial r}, \quad U_\theta = \frac{1}{r}\frac{\partial\phi^f}{\partial\theta} - \frac{\partial\psi^f}{\partial r}, \end{aligned} \quad (15)$$

where $\phi^s = \phi^s_1 + \phi^s_2$, $\phi^f = \phi^f_1 + \phi^f_2 = \mu_1\phi^s_1 + \mu_2\phi^s_2$. Also, the general stress-strain relations in the Biot theory are given by [41]

$$\begin{aligned} \sigma^s_{ij} &= \left[(P-2N)e + Q\varepsilon\right]\delta_{ij} + 2Ne^s_{ij}, \\ \sigma^f_{ij} &= -\phi_0 p_p\delta_{ij} = (Qe + R\varepsilon)\delta_{ij}, \end{aligned} \quad (16)$$

where δ_{ij} is the Kronecker delta function, $e^s_{ij} = (u_{i,j} + u_{j,i})/2$, p_p is the acoustic pore fluid pressure, and using (10) and (11) the appropriate expressions for the frame and fluid dilatations can be determined from

$$\begin{aligned} e &= \nabla\cdot\boldsymbol{u} = \nabla^2\phi^s = \nabla^2\phi^s_1 + \nabla^2\phi^s_2 \\ &= -k^2_1\phi^s_1 - k^2_2\phi^s_2, \\ \varepsilon &= \nabla\cdot\boldsymbol{U} = \nabla^2\phi^f = \mu_1\nabla^2\phi^s_1 + \mu_2\nabla^2\phi^s_2 \\ &= -\mu_1k^2_1\phi^s_1 - \mu_2k^2_2\phi^s_2, \end{aligned} \quad (17)$$

Subsequent use of (17) in (16), the general expressions for the relevant stress components and the pore fluid pressure are readily derived as

$$\begin{aligned} \sigma^s_{rr} &= a_1k^2_1\phi^s_1 + a_2k^2_2\phi^s_2 + 2N\frac{\partial u_r}{\partial r}, \\ \sigma^s_{r\theta} &= \frac{N}{r}\left(\frac{\partial u_r}{\partial\theta} + r\frac{\partial u_\theta}{\partial r} - u_\theta\right), \\ \phi_0 p_p &= b_1k^2_1\phi^s_1 + b_2k^2_2\phi^s_2, \end{aligned} \quad (18)$$

where $a_{1,2} = 2N - P - Q\mu_{1,2}$ and $b_{1,2} = Q + R\mu_{1,2}$.

At this point, the field expansions for the fast and slow dilatational waves, and the shear wave transmitted into the poroelastic coating may be expressed in the general form

$$\begin{aligned} \phi^s_1 &= \sum_{n=-\infty}^{\infty}\left[B_n(\omega)J_n(k_1r_1)\mathrm{e}^{\mathrm{i}n\theta_1} + C_n(\omega)H_n(k_1r_2)\mathrm{e}^{\mathrm{i}n\theta_2}\right], \\ \phi^s_2 &= \sum_{n=-\infty}^{\infty}\left[D_n(\omega)J_n(k_2r_1)\mathrm{e}^{\mathrm{i}n\theta_1} + E_n(\omega)H_n(k_2r_2)\mathrm{e}^{\mathrm{i}n\theta_2}\right], \\ \psi^s &= \sum_{n=-\infty}^{\infty}\left[F_n(\omega)J_n(k_3r_1)\mathrm{e}^{\mathrm{i}n\theta_1} + G_n(\omega)H_n(k_3r_2)\mathrm{e}^{\mathrm{i}n\theta_2}\right], \end{aligned} \quad (19)$$

where we note that the last (first) terms in each of the above equations are expressed in the second (first) coordinate systems. These terms have to be transformed to the first (second) coordinate system before imposing the boundary conditions. Moreover, the field expansions in the cylindrical core may be represented by

$$\begin{aligned} \tilde{\phi}^s_1(r_2, \theta_2, \omega) &= \sum_{n=-\infty}^{\infty} K_n(\omega)J_n(\tilde{k}_1r_2)\mathrm{e}^{\mathrm{i}n\theta_2}, \\ \tilde{\phi}^s_2(r_2, \theta_2, \omega) &= \sum_{n=-\infty}^{\infty} L_n(\omega)J_n(\tilde{k}_2r_2)\mathrm{e}^{\mathrm{i}n\theta_2}, \\ \tilde{\psi}^s(r_2, \theta_2, \omega) &= \sum_{n=-\infty}^{\infty} M_n(\omega)J_n(\tilde{k}_3r_2)\mathrm{e}^{\mathrm{i}n\theta_2}, \end{aligned} \quad (20)$$

where the overscript "tilda" refers to the parameters associated with the poroelastic core, and the unknown scattering coefficients $A_n(\omega)$ through $M_n(\omega)$ will be determined next by imposing the suitable boundary conditions.

2.3. Boundary conditions and wave transformations

Many radiation and scattering problems involve waves of one characteristic shape (coordinate system) that are incident upon a boundary of some other shape (coordinate system). So it is difficult to satisfy the boundary conditions on that surface. There exists, however, a class of mathematical relationships called wave transformations (addition theorems) that circumvents this difficulty in many cases by allowing one to study the fields scattered by the various interfaces, all referred to a common origin. The specific boundary conditions that have to be satisfied for the poroelastic coating in contact with the surrounding acoustic medium (i.e., at $r_1 = a$) are [41]

(i) the continuity of pressure, i.e., $p_p = p$.

Document downloaded by @DAEL, 2026-11-22 13:30:33 - personal use only

(ii) the compatibility of total stresses, i.e.,

$$\sigma_{rr}^{s} = -(1-\phi_0)p \quad \text{and} \quad \sigma_{r\theta}^{s} = 0,$$

(iii) the conservation of fluid volume, i.e.,

$$(1-\phi_0)\dot{u}_r + \phi_0\dot{U}_r = \dot{s}_r. \tag{21}$$

Also, at $r_2 = b$, the velocities and stresses in poroelastic coating must be equal to the same quantities in poroelastic core [41]:

$$\begin{aligned} &\dot{u}_r = \dot{\tilde{u}}_r, \quad \dot{u}_\theta = \dot{\tilde{u}}_\theta, \quad \phi_0\big(\dot{U}_r - \dot{u}_r\big) = \tilde{\phi}_0\big(\dot{\tilde{U}}_r - \dot{\tilde{u}}_r\big), \\ &\tilde{\phi}_0\sigma_{rr}^{f} = \phi_0\tilde{\sigma}_{rr}^{f}, \quad \sigma_{r\theta}^{s} = \tilde{\sigma}_{r\theta}^{s}, \quad \sigma_{rr}^{s} + \sigma_{rr}^{f} = \tilde{\sigma}_{rr}^{s} + \tilde{\sigma}_{rr}^{f}. \end{aligned} \tag{22}$$

Now, to fulfil orthogonality in the current problem, we need to express the cylindrical wave functions of the first (second) coordinate system in terms of cylindrical wave functions of the second (first) coordinate system by application of the classical form of translational addition theorem for cylindrical coordinates [45]:

$$\begin{aligned} H_n(k_i r_2)\mathrm{e}^{\mathrm{i}m\theta_2} &= \sum_{m=-\infty}^{\infty} J_{m-n}(k_i d)H_m(k_i r_1)\mathrm{e}^{\mathrm{i}m\theta_1}, \\ J_n(k_i r_1)\mathrm{e}^{\mathrm{i}m\theta_1} &= \sum_{m=-\infty}^{\infty} J_{n-m}(k_i d)J_m(k_i r_2)\mathrm{e}^{\mathrm{i}m\theta_2}, \end{aligned} \tag{23}$$

where $i = 1, 2, 3$. Subsequently, the above addition theorem may advantageously be utilized in (19) to express the field potentials in the poroelastic coating merely with respect to the first or the second coordinate system, i.e., we may either write

$$\begin{aligned} \phi_1^s(r_1,\theta_1,\omega) &= \sum_{n=-\infty}^{\infty}\Big[B_n(\omega)J_n(k_1r_1)\mathrm{e}^{\mathrm{i}n\theta_1} + C_n^*(\omega)H_n(k_1r_1)\mathrm{e}^{\mathrm{i}n\theta_1}\Big], \\ \phi_2^s(r_1,\theta_1,\omega) &= \sum_{n=-\infty}^{\infty}\Big[D_n(\omega)J_n(k_2r_1)\mathrm{e}^{\mathrm{i}n\theta_1} + E_n^*(\omega)H_n(k_2r_1)\mathrm{e}^{\mathrm{i}n\theta_1}\Big], \\ \psi^s(r_1,\theta_1,\omega) &= \sum_{n=-\infty}^{\infty}\Big[F_n(\omega)J_n(k_3r_1)\mathrm{e}^{\mathrm{i}n\theta_1} + G_n^*(\omega)H_n(k_3r_1)\mathrm{e}^{\mathrm{i}n\theta_1}\Big], \end{aligned} \tag{24}$$

or

$$\begin{aligned} \phi_1^s(r_2,\theta_2,\omega) &= \sum_{n=-\infty}^{\infty}\Big[B_n^*(\omega)J_n(k_1r_2)\mathrm{e}^{\mathrm{i}n\theta_2} + C_n(\omega)H_n(k_1r_2)\mathrm{e}^{\mathrm{i}n\theta_2}\Big], \\ \phi_2^s(r_2,\theta_2,\omega) &= \sum_{n=-\infty}^{\infty}\Big[D_n^*(\omega)J_n(k_2r_2)\mathrm{e}^{\mathrm{i}n\theta_2} + E_n(\omega)H_n(k_2r_2)\mathrm{e}^{\mathrm{i}n\theta_2}\Big], \\ \psi^s(r_2,\theta_2,\omega) &= \sum_{n=-\infty}^{\infty}\Big[F_n^*(\omega)J_n(k_3r_2)\mathrm{e}^{\mathrm{i}n\theta_2} + G_n(\omega)H_n(k_3r_2)\mathrm{e}^{\mathrm{i}n\theta_2}\Big], \end{aligned} \tag{25}$$

where

$$\begin{aligned} B_n^*(\omega) &= \sum_{m=-\infty}^{\infty} B_m(\omega)J_{m-n}(k_1d), \\ C_n^*(\omega) &= \sum_{m=-\infty}^{\infty} C_m(\omega)J_{m-n}(k_1d), \\ D_n^*(\omega) &= \sum_{m=-\infty}^{\infty} D_m(\omega)J_{m-n}(k_2d), \\ E_n^*(\omega) &= \sum_{m=-\infty}^{\infty} E_m(\omega)J_{m-n}(k_2d), \\ F_n^*(\omega) &= \sum_{m=-\infty}^{\infty} F_m(\omega)J_{m-n}(k_3d), \\ G_n^*(\omega) &= \sum_{m=-\infty}^{\infty} G_m(\omega)J_{m-n}(k_3d). \end{aligned} \tag{26}$$

Subsequent utilization of the expansions (2), (3), (20), (24) and (25) in the boundary conditions (21) and (22) yield

$$\begin{aligned} &-\mathrm{i}\omega\phi_0\rho_0H_n(k\mathrm{a})A_n + b_1k_1^2J_n(k_1\mathrm{a})B_n + b_1k_1^2H_n(k_1\mathrm{a})C_n^* \\ &+ b_2k_2^2J_n(k_2\mathrm{a})D_n + b_2k_2^2H_n(k_2\mathrm{a})E_n^* \\ &\qquad = \varphi_0\omega\phi_0\rho_0\mathrm{i}^{n+1}\mathrm{e}^{-\mathrm{i}n\alpha}J_n(k\mathrm{a}), \end{aligned} \tag{27a}$$

$$\begin{aligned} &(1-\phi_0)\mathrm{i}\omega\rho_0H_n(k\mathrm{a})A_n \\ &\quad + \big[a_1k_1^2J_n(k_1\mathrm{a}) + 2Nk_1^2J_n''(k_1\mathrm{a})\big]B_n \\ &\quad + \big[a_1k_1^2H_n(k_1\mathrm{a}) + 2Nk_1^2H_n''(k_1\mathrm{a})\big]C_n^* \\ &\quad + \big[a_2k_2^2J_n(k_2\mathrm{a}) + 2Nk_2^2J_n''(k_2\mathrm{a})\big]D_n \\ &\quad + \big[a_2k_2^2H_n(k_2\mathrm{a}) + 2Nk_2^2H_n''(k_2\mathrm{a})\big]E_n^* \\ &\quad - (2\mathrm{i}nN/a^2)\big[J_n(k_3\mathrm{a}) - ak_3J_n'(k_3\mathrm{a})\big]F_n \\ &\quad - (2\mathrm{i}nN/a^2)\big[H_n(k_3\mathrm{a}) - ak_3H_n'(k_3\mathrm{a})\big]G_n^* \\ &\qquad = (\phi_0-1)\varphi_0\omega\rho_0\mathrm{i}^{n+1}\mathrm{e}^{-\mathrm{i}n\alpha}J_n(k\mathrm{a}), \end{aligned} \tag{27b}$$

$$\begin{aligned} &2\mathrm{i}nN\big[ak_1J_n'(k_1\mathrm{a}) - J_n(k_1\mathrm{a})\big]B_n \\ &\quad + 2\mathrm{i}nN\big[ak_1H_n'(k_1\mathrm{a}) - H_n(k_1\mathrm{a})\big]C_n^* \\ &\quad + 2\mathrm{i}nN\big[ak_2J_n'(k_2\mathrm{a}) - J_n(k_2\mathrm{a})\big]D_n \\ &\quad + 2\mathrm{i}nN\big[ak_2H_n'(k_2\mathrm{a}) - H_n(k_2\mathrm{a})\big]E_n^* \\ &\quad - N\big[n^2J_n(k_3\mathrm{a}) + a^2k_3^2J_n''(k_3\mathrm{a}) - ak_3J_n'(k_3\mathrm{a})\big]F_n \\ &\quad - N\big[n^2H_n(k_3\mathrm{a}) + a^2k_3^2H_n''(k_3\mathrm{a}) - ak_3H_n'(k_3\mathrm{a})\big]G_n^* \\ &\qquad = 0, \end{aligned} \tag{27c}$$

$$\begin{aligned} &-kH_n'(k\mathrm{a})A_n + \mathrm{i}\omega k_1(\phi_0 - \phi_0\mu_1 - 1)J_n'(k_1\mathrm{a})B_n \\ &\quad + \mathrm{i}\omega k_1(\phi_0 - \phi_0\mu_1 - 1)H_n'(k_1\mathrm{a})C_n^* \\ &\quad + \mathrm{i}\omega k_2(\phi_0 - \phi_0\mu_2 - 1)J_n'(k_2\mathrm{a})D_n \\ &\quad + \mathrm{i}\omega k_2(\phi_0 - \phi_0\mu_2 - 1)H_n'(k_2\mathrm{a})E_n^* \\ &\quad + (n\omega/a)(\phi_0\mu_3 - \phi_0 + 1)J_n(k_3\mathrm{a})F_n \\ &\quad + (n\omega/a)(\phi_0\mu_3 - \phi_0 + 1)H_n(k_3\mathrm{a})G_n^* \\ &\qquad = \varphi_0k\mathrm{i}^n\mathrm{e}^{-\mathrm{i}n\alpha}J_n'(k\mathrm{a}), \end{aligned} \tag{27d}$$

$$\begin{aligned} &k_1J_n'(k_1b)B_n^* + k_1H_n'(k_1b)C_n + k_2J_n'(k_2b)D_n^* \\ &\quad + k_2H_n'(k_2b)E_n + \mathrm{i}(n/b)J_n(k_3b)F_n^* \\ &\quad + \mathrm{i}(n/b)H_n(k_3b)G_n - \tilde{k}_1J_n'(\tilde{k}_1b)K_n \end{aligned} \tag{27e}$$

Document downloaded by @DAEL, 2026-11-22 13:30:33 - personal use only

Table I. Parameter values used in calculations.

Elastic frame parameter	Plastic foam (PF)	Light glass wool (LGW)	Saturating fluid (air)
ρ_1 (kg/m^3)	33	41	$T = 300$ K
N (N/m^2)	$(1 + 0.1\mathrm{i}) \cdot 10^6$	$(22 + 2.2\mathrm{i}) \cdot 10^4$	$p_0 = 1.0 \cdot 10^5$ Pa
ν	0.3	0	$c_0 = 346.2$ m/s
ϕ_0	0.98	0.99	$\rho_0 = 1.18$ kg/m^3
α_∞	1.4	1	$Pr = 0.70$
σ (Ns/m^4)	$5 \cdot 10^4$	9000	$\eta = 1.83 \cdot 10^{-5}$ kg/m s
Λ (m)	$1.51 \cdot 10^{-4}$	$1.92 \cdot 10^{-4}$	$\gamma = 1.4$
Λ' (m)	$2.18 \cdot 10^{-4}$	$3.84 \cdot 10^{-4}$	

$$
\begin{aligned}
&- \tilde{k}_2 J_n'(\tilde{k}_2 b) L_n - \mathrm{i}(n/b) J_n(\tilde{k}_3 b) M_n = 0, \\
&\mathrm{i}nJ_n(k_1 b) B_n^* + \mathrm{i}nH_n(k_1 b) C_n + \mathrm{i}nJ_n(k_2 b) D_n^* \\
&\quad + \mathrm{i}nH_n(k_2 b) E_n - bk_3 J_n'(k_3 b) F_n^* + bk_3 H_n'(k_3 b) G_n \\
&\quad - \mathrm{i}nJ_n(\tilde{k}_1 b) K_n - \mathrm{i}nJ_n(\tilde{k}_2 b) L_n \qquad (27\mathrm{f}) \\
&\qquad + b\tilde{k}_3 J_n'(\tilde{k}_3 b) M_n = 0, \\
&\left[a_1 k_1^2 J_n(k_1 b) + 2Nk_1^2 J_n''(k_1 b) - b_1 k_1^2 J_n(k_1 b)\right] B_n^* \\
&\quad + \left[a_1 k_1^2 H_n(k_1 b) + 2Nk_1^2 H_n''(k_1 b) - b_1 k_1^2 H_n(k_1 b)\right] C_n \\
&\quad + \left[a_2 k_2^2 J_n(k_2 b) + 2Nk_2^2 J_n''(k_2 b) - b_2 k_2^2 J_n(k_2 b)\right] D_n^* \\
&\quad + \left[a_2 k_2^2 H_n(k_2 b) + 2Nk_2^2 H_n''(k_2 b) - b_2 k_2^2 H_n(k_2 b)\right] E_n \\
&\quad + (2\mathrm{i}nN/b^2)\left[- J_n(k_3 b) + bk_3 J_n'(k_3 b)\right] F_n^* \\
&\quad + (2\mathrm{i}nN/b^2)\left[- H_n(k_3 b) + bk_3 H_n'(k_3 b)\right] G_n \qquad (27\mathrm{g}) \\
&\quad + \left[- \tilde{a}_1 \tilde{k}_1^2 J_n(\tilde{k}_1 b) - 2\tilde{N}\tilde{k}_1^2 J_n''(\tilde{k}_1 b) + \tilde{b}_1 \tilde{k}_1^2 J_n(\tilde{k}_1 b)\right] K_n \\
&\quad + \left[- \tilde{a}_2 \tilde{k}_2^2 J_n(\tilde{k}_2 b) - 2\tilde{N}\tilde{k}_2^2 J_n''(\tilde{k}_2 b) + \tilde{b}_2 \tilde{k}_2^2 J_n(\tilde{k}_2 b)\right] L_n \\
&\qquad + (2\mathrm{i}n\tilde{N}/b^2)\left[J_n(\tilde{k}_3 b) + b\tilde{k}_3 J_n'(\tilde{k}_3 b)\right] M_n = 0, \\
&2\mathrm{i}nN\left[bk_1 J_n'(k_1 b) - J_n(k_1 b)\right] B_n^* \\
&\quad + 2\mathrm{i}nN\left[bk_1 H_n'(k_1 b) - H_n(k_1 b)\right] C_n \\
&\quad + 2\mathrm{i}nN\left[bk_2 J_n'(k_2 b) - J_n(k_2 b)\right] D_n^* \\
&\quad + 2\mathrm{i}nN\left[bk_2 H_n'(k_2 b) - H_n(k_2 b)\right] E_n \\
&\quad - N\left[n^2 J_n(k_3 b) + b^2 k_3^2 J_n''(k_3 b) - bk_3 J_n'(k_3 b)\right] F_n^* \\
&\quad - N\left[n^2 H_n(k_3 b) + b^2 k_3^2 H_n''(k_3 b) - bk_3 H_n'(k_3 b)\right] G_n \\
&\quad - 2\mathrm{i}n\tilde{N}\left[b\tilde{k}_1 J_n'(\tilde{k}_1 b) - J_n(\tilde{k}_1 b)\right] K_n \qquad (27\mathrm{h}) \\
&\quad - 2\mathrm{i}n\tilde{N}\left[b\tilde{k}_2 J_n'(\tilde{k}_2 b) - J_n(\tilde{k}_2 b)\right] L_n \\
&\quad - \tilde{N}\left[n^2 J_n(\tilde{k}_3 b) - b^2 \tilde{k}_3 J_n''(\tilde{k}_3 b) + b\tilde{k}_3 J_n'(\tilde{k}_3 b)\right] M_n = 0, \\
&\mathrm{i}\omega k_1 \phi_0 (1 - \mu_1) J_n'(k_1 b) B_n^* + \mathrm{i}\omega k_1 \phi_0 (1 - \mu_1) H_n'(k_1 b) C_n \\
&\quad + \mathrm{i}\omega k_2 \phi_0 (1 - \mu_2) J_n'(k_2 b) D_n^* \\
&\quad + \mathrm{i}\omega k_2 \phi_0 (1 - \mu_2) H_n'(k_2 b) E_n \\
&\quad + \phi_0 (n\omega/b)(\mu_3 - 1) J_n(k_3 b) F_n^* \\
&\quad + \phi_0 (n\omega/b)(\mu_3 - 1) H_n(k_3 b) G_n \\
&\quad + \mathrm{i}\omega \tilde{k}_1 \tilde{\phi}_0 (\tilde{\mu}_1 - 1) J_n'(\tilde{k}_1 b) K_n \\
&\quad + \mathrm{i}\omega \tilde{k}_2 \tilde{\phi}_0 (\tilde{\mu}_2 - 1) J_n'(\tilde{k}_2 b) L_n \qquad (27\mathrm{i}) \\
&\quad + \tilde{\phi}_0 (n\omega/b)(1 - \tilde{\mu}_3) J_n(\tilde{k}_3 b) M_n = 0, \\
&b_1 \tilde{\phi}_0 k_1^2 J_n(k_1 b) B_n^* + b_1 \tilde{\phi}_0 k_1^2 H_n(k_1 b) C_n \\
&\quad + b_1 \tilde{\phi}_0 k_2^2 J_n(k_2 b) D_n^* + b_1 \tilde{\phi}_0 k_2^2 H_n(k_2 b) E_n \qquad (27\mathrm{j}) \\
&\quad - \tilde{b}_1 \phi_0 \tilde{k}_1^2 J_n(\tilde{k}_1 b) K_n - \tilde{b}_1 \phi_0 \tilde{k}_2^2 J_n(\tilde{k}_2 b) L_n = 0.
\end{aligned}
$$

Clearly the unknown scattering coefficients $A_n(\omega)$–$M_n(\omega)$ can be determined by solving the above linear system of equations. This completes the necessary background required for analyzing the problem. Next we consider some numerical examples.

3. Numerical results

In order to illustrate the nature and general behaviour of solution, we consider a number of specific numerical examples in this section. The ambient fluid is assumed to be air at atmospheric pressure and room temperature (ρ_0 = 1.18 kg/m^3, c_0 = 346.2 m/s). The compound cylinder with a fixed outer radius (a= 10 cm) is supposed to be fabricated from a proper combination of two common sound-absorbing materials (e.g., a permutation of plastic foam and light glass wool) with their physical and acoustic properties provided in Table I [46]. Accurate computation of cylindrical Bessel functions is achieved by employing MATLAB specialized math functions "besselh" and "besselj". Computations for derivatives of cylindrical Bessel functions were accomplished by utilizing (9.1.27) in the handbook by Abramowitz and Stegun [40]. A MATLAB code was constructed for treating boundary conditions, to determine the unknown scattering/transmission coefficients, and other relevant acoustic field quantities as a function of nondimensional frequency, $ka = \omega a(c_0$, at selected core eccentricity, $e = d/(\mathrm{a} - b)\%$. The computations were performed on a Pentium IV personal computer with a maximum truncation constant of $n_{\max} = m_{\max} = 40$ to assure convergence in the high frequency range, and also in case of high core eccentricity. The convergence of numerical solutions were systematically checked in a simple trail and error manner, by increasing the truncation constants (i.e., including higher number of modes) while looking for steadiness or stability in the numerical value of the solutions.

The most relevant acoustic field quantities are the (far-field) scattering form-function amplitude and the absorption cross section. The standard definition of the backscattering form-function amplitude is given by [47]

$$
\left| f_\infty(r_1, \theta_1 = \pi + \alpha, \omega) \right| \approx \lim_{r_1 \to \infty} \left| \sqrt{\frac{2r_1}{a}} \frac{\varphi_{\mathrm{scat}}(r_1, \theta_1, \omega}{\varphi_{\mathrm{inc}}} \right| . \qquad (28)
$$

Document downloaded by @DAEL, 2026-11-22 13:30:33 - personal use only

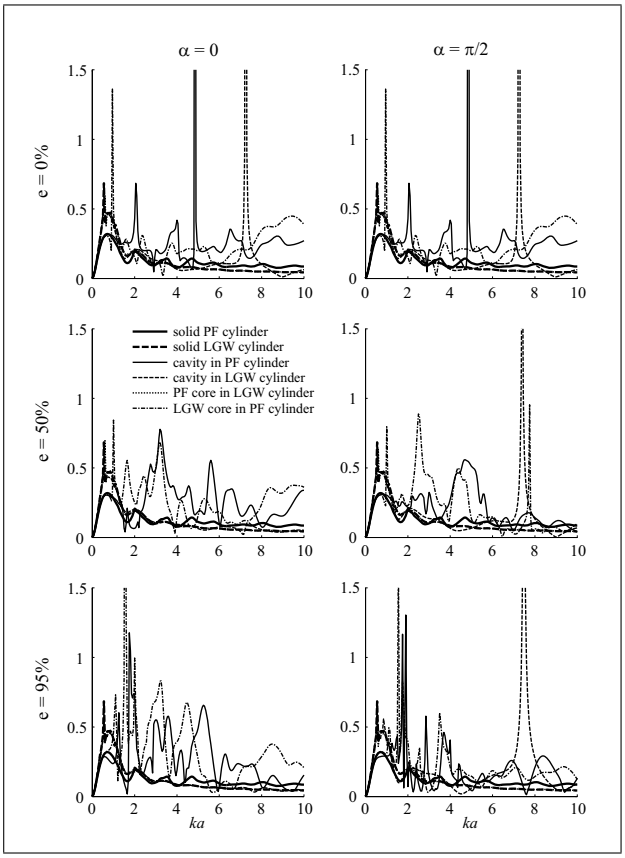


Figure 2. The variation of the back-scattered form function amplitude with dimensionless frequency for end-on/broadside incidence upon the compound cylinder at selected eccentricities and core size (b/a=0.25).

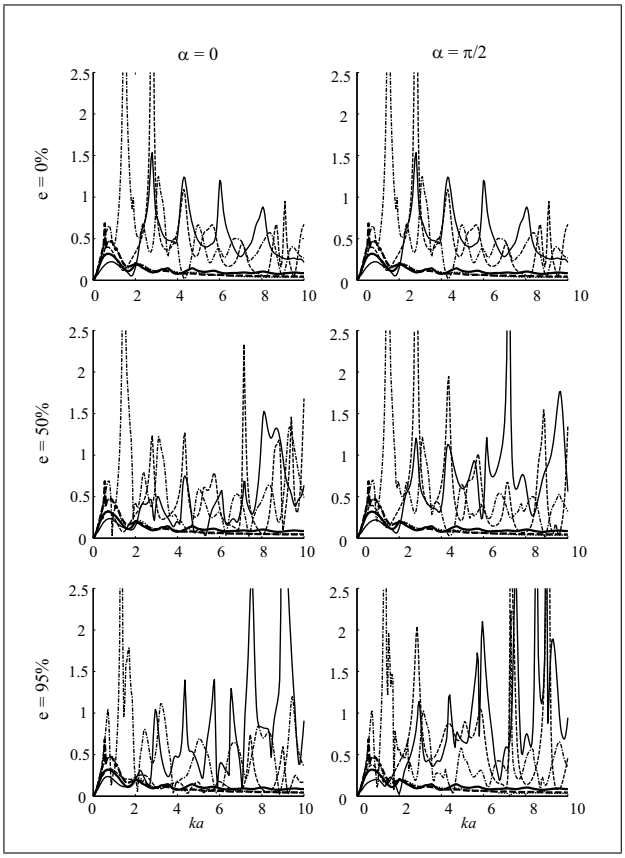


Figure 3. The variation of the back-scattered form function amplitude with dimensionless frequency for end-on/broadside incidence upon the compound cylinder at selected eccentricities and core size (b/a=0.75).

Also, the total absorption cross section is simply defined as $\sigma_{\rm abs} = \sigma_{\rm ext} - \sigma_{\rm scat}$, in which the total scattering and extinction cross sections are written as [47]

$$\sigma_{\rm scat} = \frac{4}{k\mathrm{a}} \sum_{n=-\infty}^{\infty} \left| A_n(\omega) \right|^2, \qquad (29)$$

$$\sigma_{\rm ext} = -\frac{4}{k\mathrm{a}} \Re e \left\{ \sum_{n=-\infty}^{\infty} A_n(\omega)\, \mathrm{e}^{\,in(\alpha-\pi/2)} \right\},$$

in which $\Re e$ denotes real part of a complex quantity.

The two most important incidence angles are $\alpha = 0$ (end-on) and $\alpha = \pi/2$ (broadside), as they best help to expose the physics of the problem. Figures 2 through 4 display the variation of the back-scattered form function amplitude with ka for broadside/end-on incidence upon the compound cylinder at selected eccentricities ($e = d/(\mathrm{a}-b)$ = 0, 50, 95%) and core sizes (b/a = 0.25, 0.75, 0.95). Six distinct configurations are examined, namely, a solid plastic foam absorber (solid thick line), a solid light glass wool absorber (dashed thick line), a plastic foam cylinder with an eccentric air-filled cavity (solid line), a light glass wool cylinder with an eccentric air-filled cavity (dashed line), a plastic foam core eccentrically embedded in a light glass wool cylinder (dotted line), and a light glass wool core eccentrically embedded in a plastic foam cylinder (dash-dotted line). The form function amplitude curves associated with the solid cylinder as well as the cavity-cored cylinder were generated by using independently developed MATLAB codes. Careful examination of the figure leads to the following general remarks. The first important observation is that the effect of core eccentricity on the form function amplitude is greater in the end-on ($\alpha = 0$) incidence configuration in comparison with the broadside incidence situation ($\alpha = \pi/2$). For the compound absorber containing the smallest core (see Figure 2), the backscattering form functions associated with the solid light glass wool (LGW) cylinder perfectly coincide with those of the plastic foam (PF) core embedded in LGW cylinder (i.e., the dotted lines perfectly coincide with dashed thick lines). On the other hand, the form functions for LGW core in PF cylinder (solid black lines) are distinctively different from those of the solid PF cylinder (dash-dotted lines). Hence we may conclude that using LGW in the structure of the compound cylindrical absorber (especially as a coating) is significantly more influential on the scattered sound field than using PF material. Furthermore, in case of end-on ($\alpha = 0$) incidence upon a LGW cylinder containing a small air-filled cavity (see dashed lines in Figure 2), as we increase the eccentricity of cavity (i.e., we move the cavity in the forward direction along the incident wave), the effect of presence of the cavity gradually disappears

Document downloaded by @DAEL, 2026-11-22 13:30:33 - personal use only

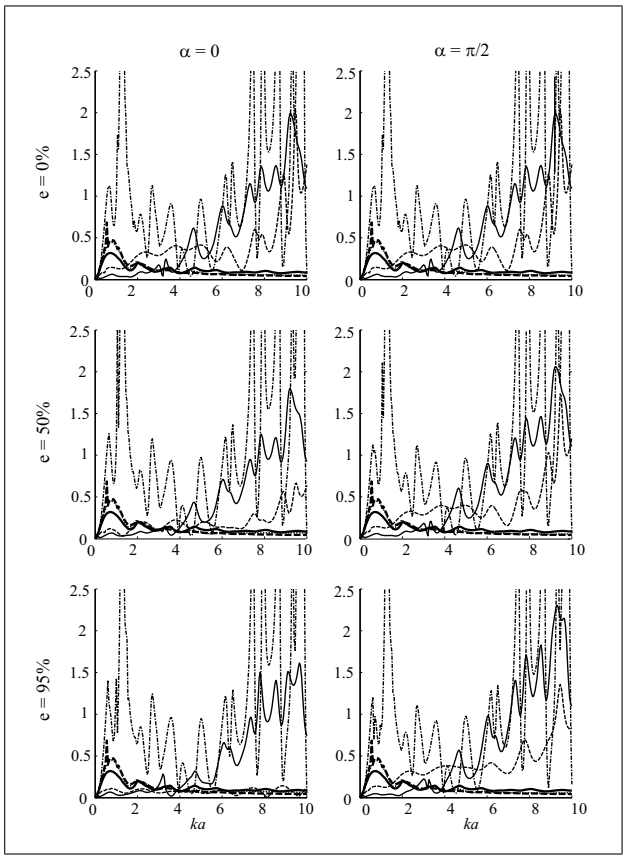


Figure 4. The variation of the back-scattered form function amplitude with dimensionless frequency for end-on/broadside incidence upon the compound cylinder at selected eccentricities and core size (b/a=0.95).

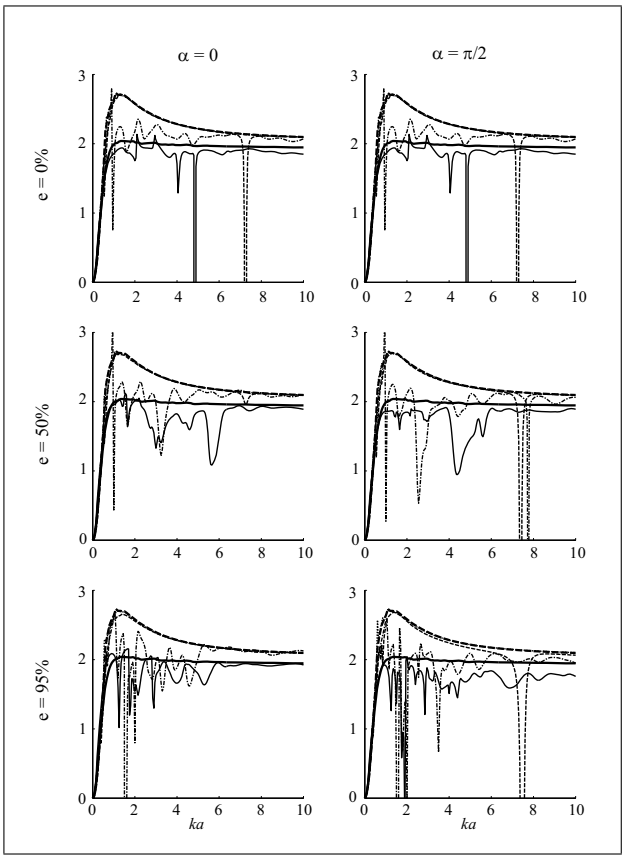


Figure 5. The variation of the total absorption cross section with non-dimensional frequency for end-on/broadside incidence upon the compound cylinder at the selected eccentricities and core size ($b/$a=0.25).

(i.e., the dashed line in the first column of Figure 2 gradually merges with the dashed thick line as the core eccentricity increases). For end-on ($\alpha = 0$) incidence upon a PF cylinder containing a small air-filled cavity (or LGW core), on the other hand, the increasing cavity (core) eccentricity leads to a notable increase in the backscattering form function amplitude.

As the compound absorber's core/cavity size increases, general observations similar the preceding discussions can readily be made. The most important distinctions are as follows. The effect of core/cavity eccentricity as well as the angle of incidence decrease as the core/cavity size increases. This is clearly due to the smaller range of possible eccentricity variations for the relatively larger core cylinder. Furthermore, the overall form function magnitudes and oscillations notably increase, especially for LGW-cored and cavity-cored compound absorbers at high incident wave frequencies. Also, as noted earlier, even for the compound absorber containing the largest core ($b/$a = 0.95; Figure 4), the backscattering form functions associated with the solid LGW cylinder (dashed thick lines) perfectly coincide with those of the compound cylinder with a PF core embedded in a very thin LGW cylinder (dotted lines). Thus we may conclude that application of a very thin LGW coating on a PF core can be very consequential on the backscattered acoustic field amplitude. Lastly, the most important observation is perhaps the fact that, while the backscattered form function amplitudes associated with the cavity-cored cylinders are relatively high at intermediate and high frequencies, they undergo a drastic decrease at low frequencies with increasing the cavity size for both PF and LGW cylinders (see solid and dashed lines in Figure 4), especially for end-on incidence at the highest eccentricity ($e = 95\%$).

In order to assess the sound absorption effects, we further examine the variation of the total absorption cross section with non-dimensional frequency for broadside/end-on incidence upon the compound cylinder at the selected eccentricities and core sizes in Figures 5 through 7. It is interesting to study the change in absorption cross section as the incident wave frequency, angle, core eccentricity and size are changed. The most important observations are as follows. The first important observation is that, in contrast to the form function plots, the effect of angle of incidence on the absorption cross sections is not generally very critical, especially as the core/cavity size increases. Furthermore, the absorption cross section curves corresponding to the solid PF cylinder (solid thick lines), the solid LGW cylinder (dashed thick lines), and the PF core in LGW cylinder (dotted lines) exhibit the most ideal sound absorption behaviour. In particular, after passing through a relatively wide peak near $ka \approx 1$, they steadily tend toward

Document downloaded by @DAEL, 2026-11-22 13:30:33 - personal use only

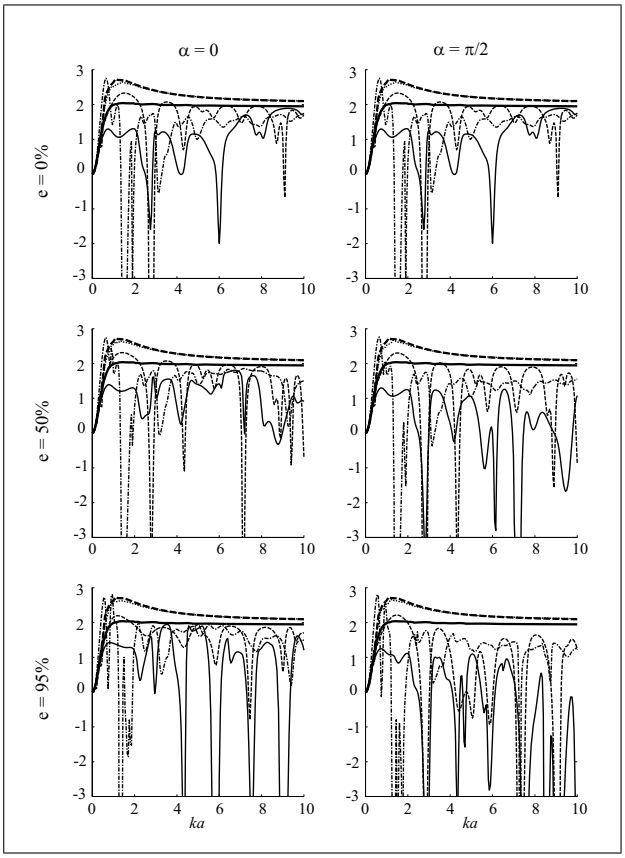


Figure 6. The variation of the total absorption cross section with non-dimensional frequency for end-on/broadside incidence upon the compound cylinder at the selected eccentricities and core size ($b/$a=0.75).

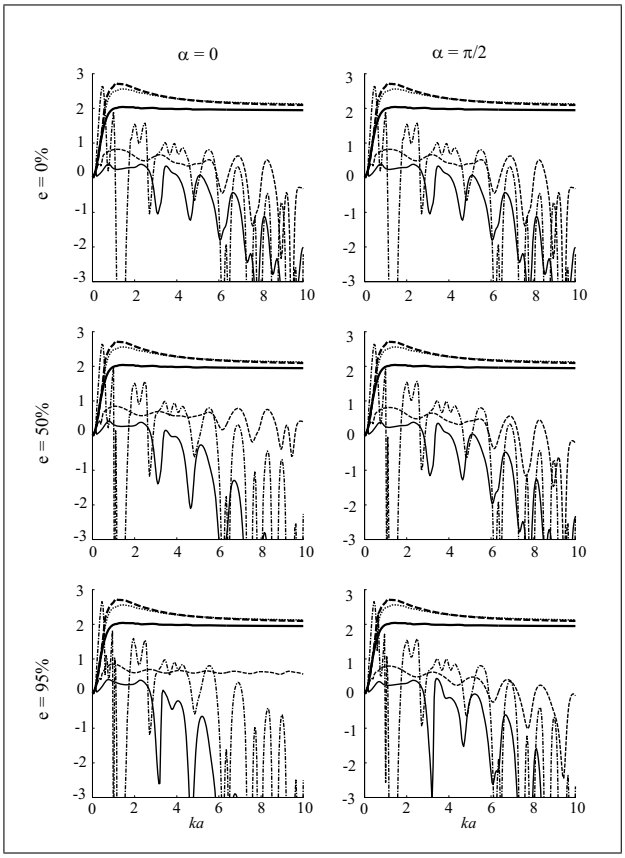


Figure 7. The variation of the total absorption cross section with non-dimensional frequency for end-on/broadside incidence upon the compound cylinder at the selected eccentricities and core size ($b/$a=0.95).

a nearly constant limit ($\sigma_{\text{abs}} \approx 2$) as the incident wave frequency increases, i.e., there are no "dips" ("peaks") in the sound absorption (associated form function) spectra. The absorption cross section curves for the remaining cases behave extremely oscillatory and possess a lot of such "deteriorative dips", especially for the larger cavity/core sizes ($b/\text{a} = 0.75, 0.95$). They tend toward the latter limit only for the smallest core/cavity size ($b/\text{a} = 0.25$), particulary for end-on incidence at the largest eccentricity ($e = 0.95\%$). In addition, the effect of core eccentricity on the absorption cross section is slightly greater in the end-on incidence configuration in comparison with the broadside incidence situation. For the compound absorber containing the smallest core (see Figure 5), the absorption cross sections associated with the solid LGW cylinder roughly coincide with those of the PF core embedded in LGW cylinder (i.e., the dotted lines perfectly coincide with dashed thick lines), nearly regardless of core size and eccentricity. Furthermore, in case of end-on incidence upon a LGW cylinder containing a small air-filled cavity ($b/\text{a} = 0.25$), the effect of presence of the cavity vanishes as we increase its eccentricity. In particular, we note that the relatively large dip in the dashed curve in the first plot of Figure 5 disappears as the core eccentricity is increased to $e = 95\%$. Lastly, the most interesting observation is perhaps the fact that, as displayed by the dotted line in Figure 7, one can achieve fairly good sound absorption by applying a thin coating layer of a superior sound absorbent material (LGW) on the surface of an inferior sound absorbing core (PF). We also note that in the end-on incidence case in Figure 7 (first column), the extremely oscillatory absorption spectra associated with the cavity in LGW cylinder (dashed line) promptly disappears as the cavity eccentricity is increased to e=95%.

Finally, in order to check overall validity of the calculations, we first used the "all-fluid approximation" [48] to compute the total scattering cross section ($k\text{a}\sigma_{\text{scat}}$) versus angle of incidence at selected radii ratios ($b/\text{a} = 0$, 0.005, 0.01) and eccentricity ($d/\text{a} = 0.6$) for an inviscid compound fluid cylinder immersed in surrounding water [26], by setting $\rho_0 = 1000\,\text{kg/m}^3$, $c_0 = 1485\,\text{m/s}$, $\phi_0^{\text{core,coating}} \to 1$, $\eta^{\text{core,coating}} \to 0$, $\rho^{\text{coating}}/\rho_0 = 1.22$, $\rho^{\text{core}}/\rho_0 = 2.7$, $k/k_2 =$ (speed of sound in the "all-fluid" coating$/c_0$) $= 1.27$, and $k/\tilde{k}_2 =$ (speed of sound in the "all-fluid" core$/c_0$) $= 4.3$ in our general MATLAB code.

The numerical results, as shown in Figure 8a, accurately perfectly reproduce the curves displayed in Figure 9b of [26]. The remaining numerical results appearing in the latter reference were also readily reproduced (not shown for briefness) by using similar limiting input parameter values in our general code. As a further check, we used the "all-solid approximation" [49] to compute the backscattered

Document downloaded by @DAEL, 2026-11-22 13:30:33 - personal use only

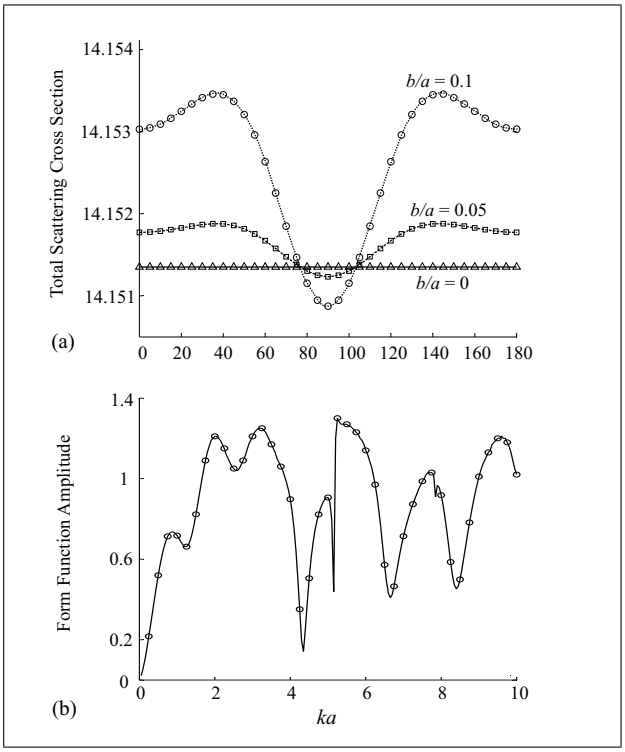


Figure 8. a. The total scattering cross section versus angle of incidence at selected radii ratios and eccentricity ($d/\mathrm{a} = 0.6$) for an inviscid compound fluid cylinder immersed in an infinite ideal fluid medium. Lines: all-fluid approximation, symbols: Roumeliotis and Kakogianno's result [26]. b. The backscattered form function amplitude versus nondimensional frequency for normal incidence upon a copper-clad (concentric) aluminium rod immersed in water. —— all-solid approximation, ◯ Honarvar and Sinclair's result [50].

form function amplitude, $|f_\infty(r_1, \theta_1 = \pi + \alpha, \omega)|$, versus nondimensional frequency for normal incidence upon a copper-clad (concentric) aluminium rod immersed in water by setting $\phi_0 \to 0$, $\alpha_\infty \to \infty$, $d = 0$, $\rho_1 = \rho_{\text{copper}}$, $\tilde{\rho}_1 = \rho_{\text{aluminum}}$, $N = G_{\text{copper}}$ and $\tilde{N} = G_{\text{aliminum}}$ in our general MATLAB code (G denotes shear modulus and physical properties of the clad rod are assumed as in Table I in [50]). The outer radius of the clad rod is taken as a= 0.915 and its core radius is $b = 0.87$ cm. Figure 8b demonstrates that our numerical results closely follow the numerical data extracted from Figure 2 of [50].

4. Conclusions

This work presents analytical solutions as well as numerical results for scattering and absorption of plane sound waves by a porous elastic compound cylindrical absorber suspended in air. The solution is based on the translational addition theorem for cylindrical wave functions and the Biot model for dynamic description of poroelastic material behaviour. The far-field backscattered form function amplitude and the absorption cross section spectra are computed for selected sound absorbent coating/core material combinations, angles of incidence, incident wave frequencies, core sizes and eccentricities. The numerical results reveal that the effect of core eccentricity on the form function amplitude is more prominent in the end-on ($\alpha = 0$) incidence configuration in comparison with the broadside incidence situation ($\alpha = \pi/2$). It has also been found that using the light glass wool (LGW) sound absorbent material in the structure of the compound cylindrical absorber (especially as a coating) is significantly more influential on the scattered sound field than using the plastic foam (PF) material. In particular, it is shown that application of a very thin LGW coating on a PF core can be very consequential on the backscattered acoustic field amplitude. The effects of core/cavity eccentricity as well as the angle of incidence decrease as the core/cavity size increases. In case of end-on incidence upon a LGW cylinder containing a small air-filled cavity, the impact of presence of the cavity gradually disappears as its eccentricity is increased. Furthermore, while the backscattered form function amplitudes associated with the cavity-cored cylinders are relatively high at intermediate and high frequencies, they undergo a drastic drop in overall magnitude at low frequencies with increasing the cavity size for both PF and LGW cylinders, especially for end-on incidence at maximum cavity eccentricity. The absorption cross section curves corresponding to the solid cylindrical absorbers (PF and LGW) as well as those of the PF-cored LGW cylinder exhibit the most ideal (wide-band) sound absorption behaviour. The absorption cross section spectra for the remaining cases behave extremely oscillatory and exhibit plenty of "deteriorative dips," especially as the cavity or core size increases. It has also been demonstrated that a fairly good sound absorption can be achieved by applying only a thin coating layer of a superior sound absorbent material (LGW) on the surface of an inferior sound absorbing core (PF). Moreover, in the end-on incidence situation, the extremely oscillatory absorption spectra associated with presence of a large cavity in LGW cylinder promptly disappears as its eccentricity is increased. Besides, it has been illustrated that nearly regardless of cavity eccentricity, the hollow (cavity-cored) cylinders are inefficient absorbers of sound energy in the intermediate and high frequency range. The proposed model is of noble interest due to its practical value in noise control engineering in addition to its inherent significance as a canonical problem in structural acoustics.

References

[1] Lord Rayleigh: Theory of sound (two volumes). Dover Publications, New York, 1945.

[2] H. Sir Lamb: Hydrodynamics. Dover Publications, New York, 1945.

[3] K. Morse, P.and Ingard: Theoretical acoustics. McGraw-Hill, New York, 1968.

[4] F. G. Mitri: Acoustic backscattering form function of absorbing cylinder targets (L). J. Acoust. Soc. Am. **115** (2004) 1411–1413.

[5] F. G. Mitri: Theoretical calculation of the acoustic radiation force acting on elastic and viscoelastic cylinders placed in

Document downloaded by @DAEL, 2026-11-22 13:30:33 - personal use only

a plane standing or quasistanding wave field. Eur. Phys. J. B **44** (2005) 71–78.

[6] F. G. Mitri: Frequency dependence of the acoustic radiation force acting on absorbing cylindrical shells. Ultrasonics **43** (2005) 271–277.

[7] S. M. Hasheminejad, N. Safari: Dynamic viscoelastic effects on sound wave diffraction by spherical and cylindrical shells submerged in and filled with viscous compressible fluids. Shock and Vibration **10** (2003) 339–363.

[8] S. M. Hasheminejad, N. Safari: Acoustic scattering from viscoelastically coated spheres and cylinders in viscous fluids. J. Sound Vib. **280** (2005) 101–125.

[9] R. P. Shaw: Diffraction of waves by circular obstacles with variable impedance boundary conditions. J. Sound Vib. **38** (1975) 417–424.

[10] F. P. Mechel: Absorption cross section of absorber cylinders. J. Sound Vib. **107** (1986) 131–148.

[11] J. Laperre, W. Thys: Scattering of ultrasonic waves by an immersed porous cylinder. Acoustics Letters **16** (1992) 9.

[12] Y. Liu: Scattering of elastic wave by an absorbing cylinder. Acta Automatica Sinica **24** (1998) 481–489.

[13] Y. Zhou, Y. Wang, L. Ma, T. Gao: Sound scattering by fluid-saturated porous cylinders. Acta Physica Sinica **49** (2000) 480–486.

[14] M. Ochmann, A. Homm, J. Ehrlich: Numerical calculation of acoustic scattering from a finite cylinder with locally varying surface impedance. Acta Acustica united with Acustica **89** (2003) 14–20.

[15] E. Sarradj: Multi-domain boundary element method for sound fields in and around porous absorbers. Acta Acustica united with Acustica **89** (2003) 21–27.

[16] J. G. Berryman: Scattering by a spherical inhomogeneity in a fluid-saturated porous medium. J. Math. Phys. **26** (1985) 1408–1419.

[17] P. M. Reddy, M. Tajuddin: Exact analysis of the plane-strain vibrations of thick walled hollow poroelastic cylinders. Int. J. Solids Struct. **37** (2000) 3439–3456.

[18] R. P. Shaw, G. Tai: Time harmonic acoustic radiation from nonconcentric circular cylinder. J. Acoust. Soc. Am. **56** (1974) 1437–1443.

[19] I. N. Kanevskii, B. S. Surikov: Two-layer acoustic lenses. Acoustics **22** (1976) 292–294.

[20] J. M. Reese, W. Thompson: Acoustic diffraction by a variable thickness fluid layer. J. Acoust. Soc. Am. **80** (1986) 1810–1815.

[21] V. B. Poruchikov, A. V. Stepanov: Diffraction of an acoustic wave by a cylinder covered by a layer of soft material. Fluid Mechanics, Soviet Research **16** (1987) 63–70.

[22] J. Sinai, R. C. Waag: Ultrasonic scattering by two concentric cylinders. J. Acoust. Soc. Am. **83** (1988) 1728–1735.

[23] G. T. Schuster: A fast exact numerical solution for the acoustic response of concentric cylinders with penetrable interfaces. J. Acoust. Soc. Am. **1990** (87) 495–502.

[24] P. J. Janele, A. Mioduchowski, J. B. Haddow: A note on finite dynamic deformation of concentric cylinders. Int. J. Eng. Sci. **29** (1991) 1585–1592.

[25] S. Morse, Z. W. Feng, P. L. Marston: High-frequency threshold processes for leaky waves on cylinders of variable thickness: Fluid shell case. J. Acoust. Soc. Am. **98** (1995) 2928.

[26] J. A. Roumeliotis, B. Kakogiannos: Acoustic scattering from an infinite cylinder of small radius coated by a penetrable one. J. Acoust. Soc. Am. **97** (1995) 2074–2081.

[27] E. B. Danila, J. M. Conoir, J. L. Izbicki: Generalized Debye series expansion: Treatment of the concentric and nonconcentric cylindrical fluid-fluid interfaces. J. Acoust. Soc. Am. **98** (1995) 3326.

[28] E. B. Danila, J. M. Conoir, J. L. Izbicki: Generalized Debye series expansion. Part II, Treatment of eccentric fluid-solid cylindrical interfaces. Acta Acustica united with Acustica **84** (1998) 38–44.

[29] S. M. Hasheminejad, M. Azarpeyvand: Energy distribution and radiation loading of a cylindrical source suspended within a nonconcentric fluid cylinder. Acta Mechanica **164** (2003) 15–30.

[30] O. Umnova, K. Attenborough, C. M. Linton: Effects of porous covering on sound attenuation by periodic arrays of cylinders. J. Acoust. Soc. Am. **119** (2006) 278–284.

[31] S. M. Hasheminejad, R. Avazmohammadi: Acoustic diffraction by a pair of poroelastic cylinders. ZAMM **86** (2006) 589–605.

[32] Z. Zhong, K. H. Wang: Solitary wave interaction with a concentric porous cylinder system. Ocean Engineering **33** (2006) 927–949.

[33] R. D. Bloebaum, K. N. Bachus, N. G. Momberger, A. A. Hofmann: Mineral apposition rates of human cancellous bone at the interface of porous coated implants. J. Biomed. Mater Res. **28** (1994) 537–544.

[34] R. H. Leland, A. A. Hofmann, K. N. Bachus, R. D. Bloebaum: Biocompatibility and bone response of human osteoarthritic cancellous bone to a titanium porous coated cobalt chromium cylinder. Transactions of the Annual Meeting of the Society for Biomaterials in conjunction with the International Biomaterials Symposium **14** (1991) 153.

[35] A. A. Hofmann: Response of human cancellous bone to identically structured commercially pure titanium and cobalt chromium alloy porous-coated cylinders. Clinical Materials **14** (1993) 101–115.

[36] A. J. T. Clemow, A. M. Weinstein, J. J. Klawitter, J. Koeneman, J. Anderson: Interface mechanics of porous titanium implants. J. Biomed. Mater Res. **15** (1981) 73–82.

[37] C. H. Bruneau, I. Mortazavi: Passive control of the flow around a square cylinder using porous media. Int. J. Numer. Meth. Fluids **46** (2004) 415–433.

[38] A. Fedorov, A. Shiplyuk, A. Maslov, E. Burov, N. Malmuth: Stabilization of a hypersonic boundary layer using an ultrasonically absorptive coating. J. Fluid Mech. **479** (2003) 99–24.

[39] V. B. Poruchikov, A. V. Stepanov: Diffraction of an acoustic wave by a cylinder covered by a layer of soft material. Fluid Mechanics, Soviet Research **16** (1987) 63–70.

[40] M. Abramovitz, I. A. Stegun: Handbook of mathematical functions. National Bureau of Standards, Washington DC, 1964.

[41] J. F. Allard: Propagation of sound in porous media: Modeling sound absorbing materials. Elsevier Applied Science, London, 1993.

[42] D. L. Johnson, J. Koplik, R. Dashen: Theory of dynamic permeability and tortuosity in fluid-saturated porous media. J. Fluid Mech. **76** (1987) 379–402.

[43] F. Luppe, J. M. Conoir, H. Franklin: Scattering by a fluid cylinder in a porous medium: Application to trabecular bone. J. Acoust. Soc. Am. **111** (2002) 2573– 2582.

[44] J. D. Achenbach: Wave propagation in elastic solids. North-Holland, New York, 1976.

[45] J. A. Stratton: Electromagnetic theory. McGraw-Hill, New York, 1941.

Document downloaded by @DAEL, 2026-11-22 13:30:33 - personal use only

[46] AutoSEA2: Foam 2003, User's guide, theory and QA. [http://www.esi-group.com/].

[47] V. V. Varadan, A. Lakhtakia, V. K. Varadan: Field representations and introduction to scattering. North-Holland, Amsterdam, 1990.

[48] S. M. Hasheminejad, H. Hosseini: Radiation loading of a cylindrical source in a fluid-filled cylindrical cavity embedded within a fluid-saturated poroelastic medium. J. Applied Mechanics **69** (2002) 675–683.

[49] S. M. Hasheminejad, S. A. Badsar: Elastic wave scattering by two spherical inclusions in a poroelastic medium. J. Engineering Mechanics **131** (2005) 953–965.

[50] F. Honarvar, A. N. Sinclair: Scattering of an obliquely incident plane wave from a circular clad rod. J. Acoust. Soc. Am. **102** (1997) 41–48.

Document downloaded by @DAEL, 2026-11-22 13:30:33 - personal use only